Visible-Near Infrared Absorbing Polymers Containing Thienoisoindigo and Electron-Rich Units for Organic Transistors with Tunable Polarity

Gitish K. Dutta, A-Reum Han, Junghoon Lee, Yiho Kim, Joon Hak Oh,* and Changduk Yang*

Systematic creation of polymeric semiconductors from novel building blocks is critical for improving charge transport properties in organic field-effect transistors (OFETs). A series of ultralow-bandgap polymers containing thienoisoindigo (TIIG) as a thiophene analogue of isoindigo (IIG) is synthesized. The UV-Vis absorptions of the TIIG-based polymers (PTIIG-T, PTIIG-Se, and PTIIG-DT) exhibit broad bands covering the visible to near-infrared range of up to 1600 nm. All the polymers exhibit unipolar p-channel operations with regard to gold contacts. PTIIG-DT with centrosymmetric donor exhibits a maximum mobility of 0.20 cm^2 V^{-1} s^{-1} under gold contacts, which is higher than those of the other polymers containing axisymmetric donors. Intriguingly, OFETs fabricated with aluminum electrodes show ambipolar charge transport with hole and electron mobilities of up to 0.28 (PTIIG-DT) and 0.03 (PTIIG-T) cm^2 V^{-1} s^{-1}, respectively. This is a record value for the hitherto reported TIIG-based OFETs. The finding demonstrates that TIIG-based polymers can potentially function as either unipolar or ambipolar semiconductors without reliance on the degree of electron affinity of the co-monomers.

1. Introduction

Organic field-effect transistors (OFETs) based on π-conjugated polymers have been the subject of intense research in the past decades because of their high potential in low-cost, large-area, and flexible devices by means of ink-jet printing and roll-to-roll manufacturing.[1] Among state-of-the-art polymeric materials for OFETs, thienyl-substituted diketopyrrolopyrrole (TDPP, **Figure 1**)-based polymers have received tremendous attention for their promising device performance in OFETs.[2] As another emerging building block that belongs to a class of the basic DPP motif, isoindigo (IIG, Figure 1) consisting of two indolin-2-one units has been frequently investigated for constructing high-performance polymer OFETs. It is believed that the incorporation of either TDPP or IIG as a strongly polar bicyclic lactam structure within the polymer backbone promotes structurally better π-stacking, thus resulting in exceptionally high charge carrier mobilities.[3] Currently, there is a keen competition between the two major rivals (TDPP vs. IIG) in the choice of the active materials for boosting OFET performance.[2c,d,f,3f,4] The protruding carbonyl groups in the TDPP not only assist fully coplanarizing the appended neighboring thiophene units through the short-contact oxygen-sulfur interactions but also the intermolecular interactions are promoted by the cross-axis dipoles.[3a,5] In the case of the IIG, however, the structural repulsion between the protons of the phenylene and the oxygen (carbonyl) of the keto-pyrrole moieties may adversely affect the stacking interactions of the polymer chains. Very recently, with a view to overcoming this drawback, Ashraf and co-workers reported the synthesis of a novel thienoisoindigo (TIIG, Figure 1) moiety by replacing the outer phenyl rings of IIG with thiophenes and its copolymer with benzothiadiazole.[6] In principle, this strategy is efficient for inducing higher planarity to the molecular plane via S···O interactions as well as to enhance the charge delocalization via a quinoidal structure of the backbone,[7] which facilitates charge carrier transport. However, TIIG-based polymeric OFETs have made very little scientific progress so far, and have reached only limited mobilities in the typical range of 10^{-4} to 10^{-1} cm^2 V^{-1} s^{-1}.[6–8] From a standpoint of the aforementioned advantages, there is room for improvement in the charge transport characteristics of TIIG-containing polymers. To address this open question, we present three TIIG-based polymers synthesized with electron-rich units such as thiophene (T),

G. K. Dutta, J. Lee, Y. Kim, Prof. C. Yang
Interdisciplinary School of Green Energy
KIER-UNIST Advanced Center for Energy
Low Dimensional Carbon Materials Center
Ulsan National Institute of Science
and Technology (UNIST)
Ulsan 689-798, South Korea
E-mail: yang@unist.ac.kr
A.-R. Han, Prof. J. H. Oh
School of Nano-Bioscience and Chemical Engineering
KIER-UNIST Advanced Center for Energy
Low Dimensional Carbon Materials Center
Ulsan National Institute of Science and Technology (UNIST)
Ulsan 689-798, South Korea
E-mail: joonhoh@unist.ac.kr

**ADVANCED
FUNCTIONAL
MATERIALS**
www.afm-journal.de
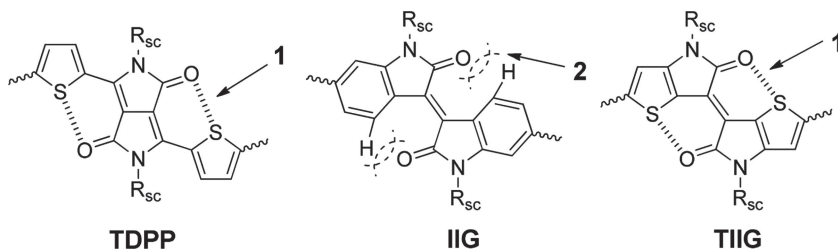
Materials Views
www.MaterialsViews.com

Figure 1. Structures of thienyl-diketopyrrolopyrrole (TDPP), isoindigo (IIG), thienoisoindigo (TIIG). 1) Conformational locking to promote π-system coplanarity via S⋯O interactions. 2) Steric hindrance between the proton of the phenyl and the carbonyl of the ketopyrrole.

selenophene (Se), or dithiophene (DT), and describe their transistor characteristics. To our delight, PTIIG-DT polymer OFETs show hole mobility of up to 0.20 cm² V⁻¹ s⁻¹, which, to the best of our knowledge, is the highest value among TIIG-based polymers reported to date. Moreover, we herein report an intriguing discovery from TIIG-containing polymers regarding electronically convertible charge transport characteristics in OFETs (from p-type to ambipolar transport), apart from the viewpoint of electron affinity of the co-monomers.
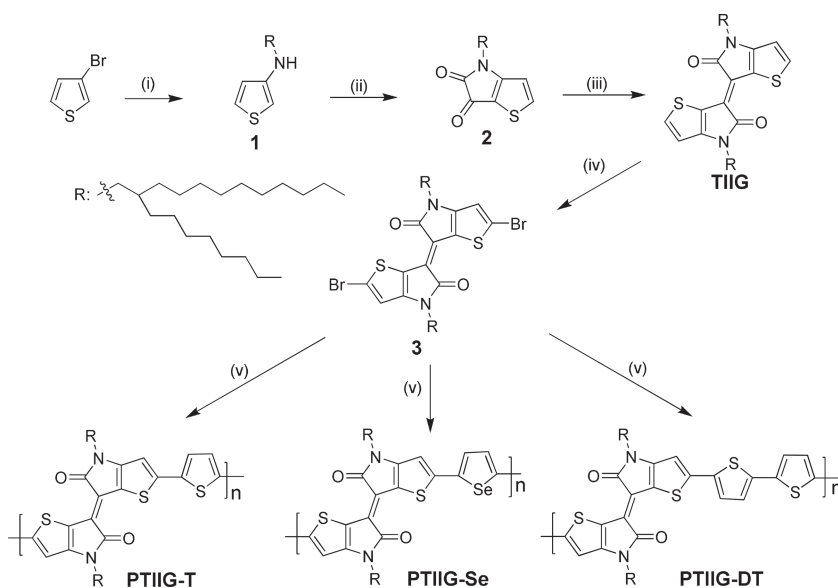
2. Results and Discussion

2.1. Synthesis and Characterization

The synthetic routes to the monomers and polymers (PTIIG-T, PTIIG-Se, and PTIIG-DT) are shown in **Scheme 1**. Starting from commercially available 3-bromothiophene, the intermediates (1 and 2) and the key material thienoisoindigo (TIIG) were synthe-

sized by the literature procedures used for the dimerization of thiophene analogue of isatin with Lawesson's reagent.[6] Followed by dibromination with NBS, TIIG was converted to 3 as a monomer for metal (Ni or Pd)-catalyzed cross-coupling polymerizations. In addition, the distannylated co-monomers such as thiophene (T), selenophene (Se), and dithiophene (DT) were easily prepared according to the established methods.[9] The polymerization was carried out under a Stille cross-coupling reaction, with 1:1 monomer ratio, using Pd₂(dba)₃ as a catalyst, and P(o-tolyl)₃ as the corresponding ligand, to give the target polymers (PTIIG-T, PTIIG-Se and PTIIG-DT) (see details in Experimental Section). After sequential Soxhlet purification with methanol, acetone, and hexane, gel-permeation chromatography (GPC) analysis against PS standard exhibits a number-averaged molecular mass (M_n) of 101.1, 76.3 and 77.1 kDa, for PTIIG-T, PTIIG-Se, and PTIIG-DT, respectively, with a polydispersity of 2.60, 2.67, and 2.08. All three polymers are readily soluble in chloroform (CF), chlorobenzene (CB) and o-dichlorobenzene (o-DCB) and form uniform thin films by spin coating. Thermogravimetric analysis (TGA) reveals good thermal stability of these polymers with decomposition temperature exceeding 387 °C (**Table 1**; Figure S1, Supporting Information).

2.2. Optical and Electrochemical Properties

Figure 2 shows the UV-Vis absorption of the TIIG-based polymers in chlorobenzene solution and as spin-coated films. Going from solution to the solid state, there are only small red-shifts (≈5 nm) of the absorption peaks, signifying that the polymers adopt similar geometries both in solution and in film. The calculated optical bandgaps from the onset absorption of the polymer thin films fall within the range of 0.89–0.97 eV, which are much smaller than those of the analogous IIG polymers.[4a,10] The difference of the optical properties between TIIG-and IIG-containing polymers is induced by the stronger electron donating properties of the thiophene ring compared to the benzene ring. Relevant data are summarized in Table 1. All polymers exhibit typically dual band absorptions both in solution and film; a sharp one at the high-energy region (350–550 nm) and a more intense, broader one at the low-energy region (700–1400 nm). Upon varying with counterpart co-monomer units (T, Se, and DT), the polymers have similar features in the high-energy bands, originating from the π–π* transition of π-conjugated backbone, while the low-energy bands induced by a typical intramolecular charge-transfer (ICT) absorption from the electron-rich to electron-deficient units are

Scheme 1. Synthetic routes to TIIG-based polymers. Reagents and conditions: (i) 2-octyldodecan-1-amine, Cu/CuI, K₃PO₄, dimethyl aminoethanol, 90 °C, 40%; (ii) oxalyl dichloride, Et₃N, DCM, 0 °C, 50%; (iii) Lawesson's reagent, toluene, 70 °C, 46%; (iv) NBS, DCM, dark, r.t., 70%; (v) 2,5-bis(trimethylstannyl)thiophene, 2,5-bis(trimethylstannyl)selenophene, or 5,5'-bis(trimethylstannyl)-2,2'-dithiophene, Pd₂(dba)₃, P(o-tolyl)₃, toluene, 110 °C, for PTIIG-T, 95%; for PTIIG-Se, 90%; for PTIIG-DT, 92%.

Materials
Views
www.MaterialsViews.com

ADVANCED
FUNCTIONAL
MATERIALS
www.afm-journal.de

FULL PAPER

Table 1. Photophysical and electrochemical properties of TIIG-based polymers.

Polymer	T_d[a] [°C]	ε [dm³mol⁻¹cm⁻¹]	$\lambda_{max}^{sol\,b)}$ [nm]	λ_{max}^{film} [nm]	$E_g^{opt\,c)}$ [eV]	E_{HOMO}[d] [eV]	E_{LUMO}[d] [eV]	$E_g^{CV\,e)}$ [eV]
PTIIG-T	395	42 500	998	998	0.91	−5.03	−3.62	1.41
PTIIG-Se	387	42 690	1050	1049	0.89	−4.95	−3.60	1.35
PTIIG-DT	401	46 410	885	887	0.97	−5.02	−3.50	1.52

a)The temperature of 5% weight-loss under nitrogen; b)Chlorobenzene solution; c)Determined from the onset of the electronic absorption spectra; d)Cyclic voltammetry determined with Fc/Fc⁺ ($E_{HOMO} = -4.80$ eV) as the external reference; e)$E_g^{CV} = E_{LUMO} - E_{HOMO}$.

significantly shifted. PTIIG-Se shows obvious red-shift of the absorption maxima compared to the other polymers, which is attributed to the increased quinoidal characteristic of the polymer backbone due to the inclusion of selenophene units. In addition, all the polymers show the high extinction coefficients that are manifested in the order of PTIIG-DT > PTIIG-Se ≥ PTIIG-T. Interestingly, in the case of PTIIG-T and PTIIG-Se, the oscillator strength of the lower-energy transitions relative to the higher-energy bands is decreased when going from solution to the solid state. In contrast, this relative strength of the two peaks for PTIIG-DT in the solid state is almost identical to that

Figure 2. UV-Vis absorption spectra of TIIG-based polymers in a) chlorobenzene solution (3.31 × 10⁻⁵ᴍ for PTIIG-T, 3.34 × 10⁻⁵ᴍ for PTIIG-Se, and 3.24 × 10⁻⁵ᴍ for PTIIG-DT) at room temperature and b) as thin-solid films (5 mg mL⁻¹, 1500 rpm for 60 s).

in solution. Through the increase of the effective conjugation length after the introduction of dithiophene units, a red-shifted absorption band for PTIIG-DT relative to PTIIG-T is predicted; however, note that λ_{max} of PTIIG-DT is remarkably blue-shifted by ≈110 nm vs. that of PTIIG-T. Other groups also reported that extending the number of thiophene rings between TDPP or IIG units led to widened the optical bandgaps.[4a,11] Although in-depth analysis and study must be required in order to gain an understanding of the unexpected chromatic shift, this may be due to the destabilization of the LUMO with successive expansion of the π-system of the thiophene moieties. This assumption is supported by both the theoretical and the experimental results (vide infra: the data from CV and DFT). In addition, we cannot rule out that the different molecular docking induced by electrostatic potentials between PTIIG-DT with centrosymmetric dithiophene and PTIIG-T with axisymmetric thiophene can cause the changed conformations in the polymer backbones.[10]

The cyclic voltammograms (CV) were used to evaluate electronic energy levels of the polymers and the electrochemical characteristics are listed in Table 1. All polymers show much stronger oxidative peaks than their reductive ones, almost one order of magnitude higher, indicating that these polymers are more easily oxidized than reduced (see **Figure 3**a). This result is consistent with the device performance, which shows all the polymers as typical p-type dominant semiconductors (vide infra). Notably, compared with the corresponding IIG analogues,[4a,10] the TIIG-based polymers have much shallow HOMO levels, due to the relative electron-rich TIIG core.

Structurally, TIIG-based polymers differ from each other based on the identity of the electron-deficient unit conjugated with, and adjacent to different donor units. Thereby, the HOMO levels with the LUMO being almost unchanged for the polymers are anticipated to vary with electron-donating properties of donor units. However, it is worth noting that both HOMO and LUMO levels are affected by the electronic structures of the donor units. For example, the HOMO/LUMO levels of PTIIG-T, PTIIG-Se, and PTIIG-DT are −5.03/−3.62 eV, −4.95/−3.60 eV, and −5.02/−3.50 eV, respectively. These results are in agreement with the computational results of the model trimeric systems using density functional theory (DFT) at the B3LYP/6-31G* with Gaussian 09 package. The molecular orbital distributions reveal that both the HOMOs and LUMOs of all the polymers are well spread over their conjugated backbones (see Figure 3b). Thereby, the nature of our TIIG polymers even with electron-rich units may be a bipolar feature with both p-type and n-type characteristics achievable by control of device architecture.
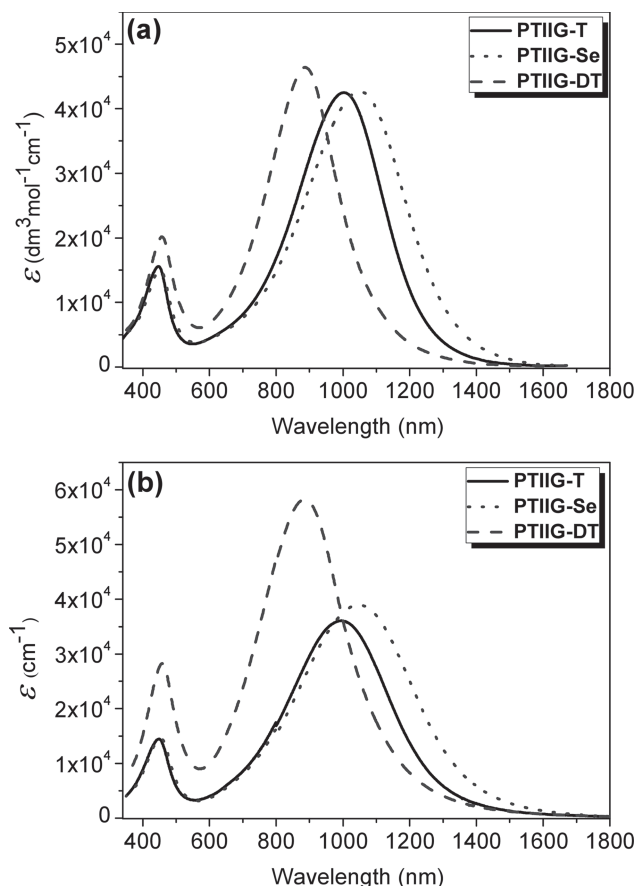
ADVANCED
FUNCTIONAL
MATERIALS
www.afm-journal.de

FULL PAPER

Materials
Views
www.MaterialsViews.com

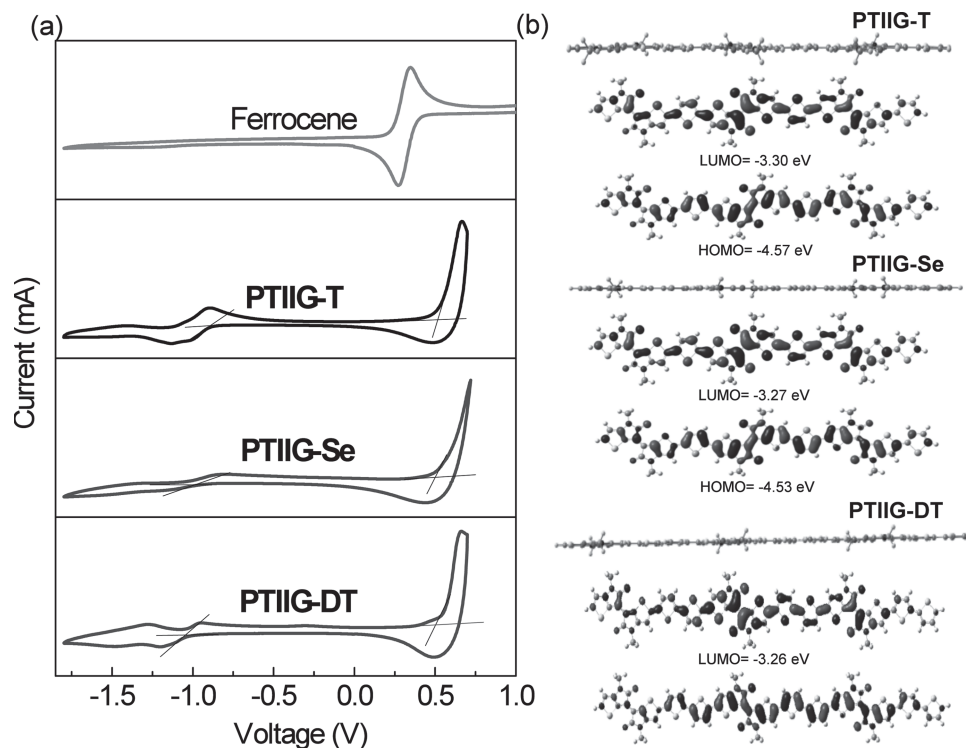**Figure 3.** a) Cyclic voltammograms of TIIG-based polymers in thin films drop-cast on a platinum working electrode and tested in n-Bu$_4$NPF$_6$/CH$_3$CN solution (scan rate, 50 mV s^{-1}). b) Calculated optimized geometries and molecular orbitals for the model trimers of TIIG-based polymers, respectively (B3LYP/6-31G*).

This is in contrast to the IIG polymer analogues with electron-rich blocks in which LUMO levels are mostly localized on the IIG core and HOMO levels are distributed along the polymer chains (for DFT calculations of the corresponding IIG polymers see Figure S2, Supporting Information).[4a,10] This implies that the electron-withdrawing effect of the TIIG group is smaller than that of IIG due to the implanted thiophene units to two lactam rings. In addition, TIIG-containing oligomers adapt perfect coplanar geometry (see Figure 3b).

To gain further insight into the structural and electronic features of the polymers, time dependent-density functional theory (TD-DFT) calculations were performed (detailed analyses in Figure S3,4 and Table S1,2 in Supporting Information). The calculated oscillator strengths (f) not only follow the same trend as the experiment results above, but also show higher values than those of the corresponding IIG analogues. It is clear that the oscillator strengths of ICT bands in the polymer backbones containing centrosymmetric DT units are larger than those of the polymers with axisymmetric donors.

2.3. OFETs Performance

To shed light on structure-property relationships in TIIG-based polymers, we fabricated bottom-gate/top-contact OFETs devices with gold (Au) as source and drain electrodes (**Figure 4**a). The polymer thin films were deposited on n-octadecyltrimethoxysilane (OTS)-treated SiO$_2$ (300 nm)/Si substrates by drop-casting

the o-DCB solution in nitrogen atmosphere (details in Experimental Section). The field-effect mobilities were extracted from the saturation regime by fitting the slope of square root drain current vs. gate voltage. **Table 2** summarizes the average and maximum mobilities for all the polymers before and after thermal annealing at 220 °C. Notably, PTIIG-T exhibits superior performance to that of a recently reported polymer (PTIIT) with the same polymer backbone.[8] This is because PTIIG-T with 2-octyldodecyl groups as larger side chains has better solubility and excellent film-forming capability. It can also be attributed to the device configuration difference, as the top-contact configuration employed for PTIIG-T OFETs generally allows larger area charge injections compared with the bottom-contact configuration used for PTIIT OFETs. The post-annealing temperature of 220 °C was chosen because PTIIG-DT exhibited the optimized performance. As expected, the as-spun thin films of all three polymers behave as p-type semiconductors with good drain-current modulation and well-defined linear and saturation regions (Figure 4b–f) and yield optimal mobilities in excess of 0.1 cm^2 V^{-1} s^{-1}. Even though selenophene-containing polymers were often reported to show a better carrier-transporting performance in OFETs than that of the thiophene-containing polymers,[2d,12] the selenophene containing polymer PTIIG-Se only shows a result comparable to those of the thiophene-containing polymers (PTIIG-T and PTIIG-DT). Very interestingly, subsequent annealing of the polymer thin films containing axisymmetric donors (PTIIG-T, PTIIG-Se) did not exhibit any mobility improvement in comparison with as-spun
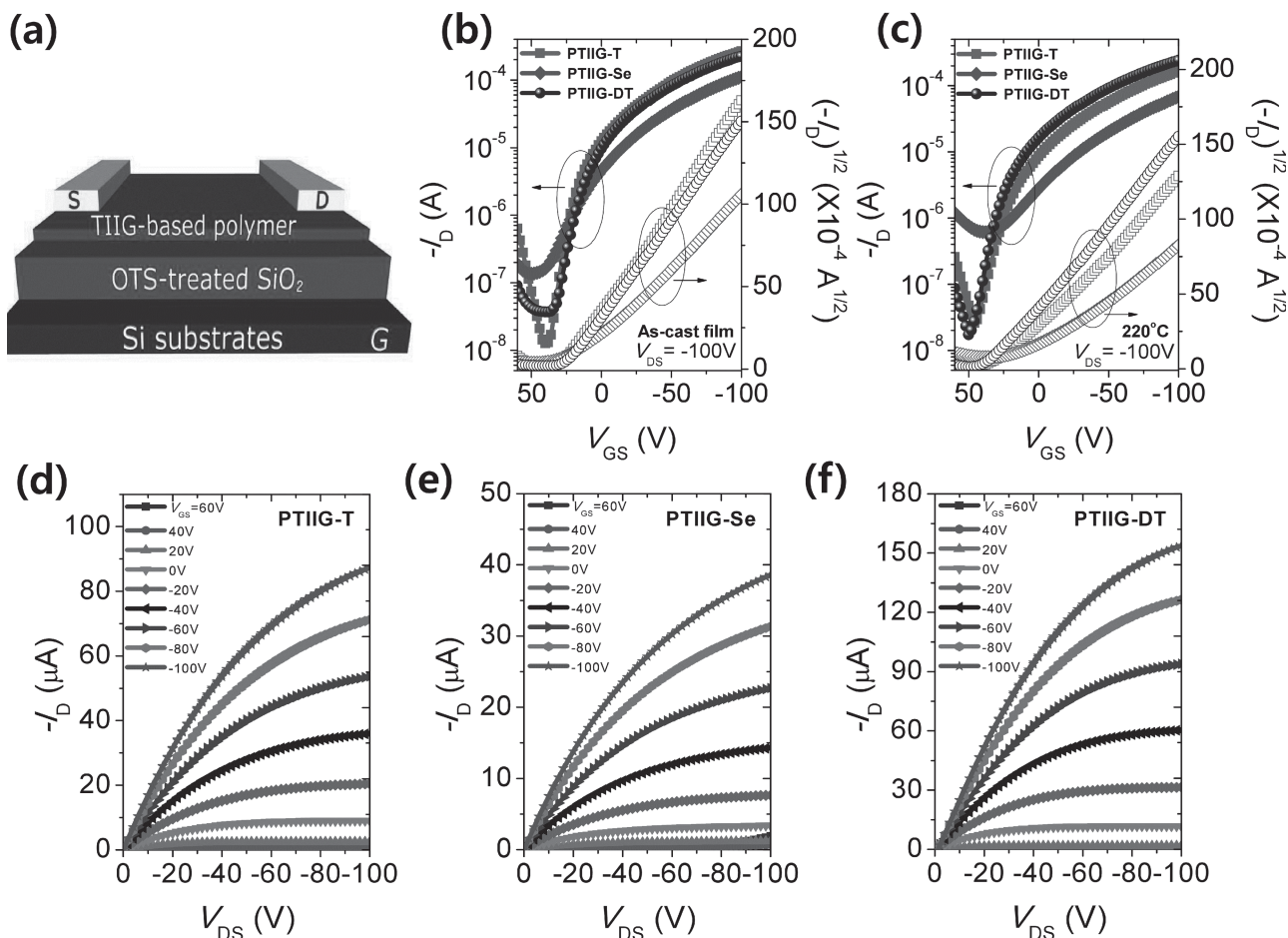
Materials
Views
www.MaterialsViews.com

ADVANCED
FUNCTIONAL
MATERIALS
www.afm-journal.de

FULL PAPER

Figure 4. a) Schematic illustration of OFETs structure. Transfer characteristics of OFET devices of TIID-based polymer films b) as-cast and c) annealed at 220 °C at hole-enhancement operation, $V_{DS} = -100$ V, with Au electrodes. Output characteristics of OFET devices of TIIG-based polymer films annealed at 220 °C with Au electrodes; d) PTIIG-T, e) PTIIG-Se, and f) PTIIG-DT.

films, whereas a trend of increased mobility upon annealing was observed in centrosymmetric PTIIG-DT, implying that a subtle change in the geometric symmetry of polymer backbones can greatly affect the thermodynamic behavior of the resulting solid-state thin film. The post-annealed PTIIG-DT thin films exhibited a maximum hole mobility of 0.20 cm^2 V^{-1} s^{-1},

Table 2. Electrical performance of OFET devices based on TIIG polymer thin films with Au contacts.

Polymer	Annealing Temp.	$\mu_{h,max}$ [cm^2 V^{-1} s^{-1}]	$\mu_{h,avg}$[a)] [cm^2 V^{-1} s^{-1}]	I_{on}/I_{off}	V_T [V]
PTIIG-T	N/A[b)]	0.17	0.15	4.6×10^2	19.4
	220 °C	0.13	0.12	3.2×10^2	18.8
PTIIG-Se	N/A	0.11	9.3×10^{-2}	3.5×10^2	18.0
	220 °C	7.9×10^{-2}	5.9×10^{-2}	3.7×10^2	5.9
PTIIG-DT	N/A	0.15	0.13	6.4×10^3	25.4
	220 °C	0.20	0.16	3.0×10^3	13.8

[a)]The average mobility of the OFET devices ($L = 50$ and $W/L = 20$); [b)]The thermal annealing was not applied (as-cast thin films).

which is the highest value among TIIG-based polymers reported to date.

It is known that the type of charge carrier in OFETs strongly depends on the variation of the electrode metals.[13] Therefore, in order to further explore the intrinsically possible polarities of TIIG-based polymers, OFETs were fabricated by replacing gold (Au) with aluminum (Al) contacts as low work-function electrodes. All the devices were annealed at 220 °C prior to testing (**Figure 5**, **Table 3**). Additionally, the attempt of intentionally changing electrode is frequently made to reduce device manufacturing costs, using cheap Al instead of expensive Au. Although all the TIID-based polymers still exhibit hole-dominant transport characteristics (the average hole mobility values are more than one order of magnitude higher than the average electron mobilities), the transfer curves trace V-shaped troughs with decreasing magnitude of the gate voltage, clearly indicating a transition from unipolar to ambipolar behaviors. Like OFETs with Au described above, PTIIG-DT showed the best hole mobility of up to 0.28 cm^2 V^{-1} s^{-1}. Until now, both the IIG and TIIG family of polymers with electron-rich units have rendered only unipolar p-type operations. In contrast, we observed, for the first time, that TIIG-based polymers even with electron-donating units
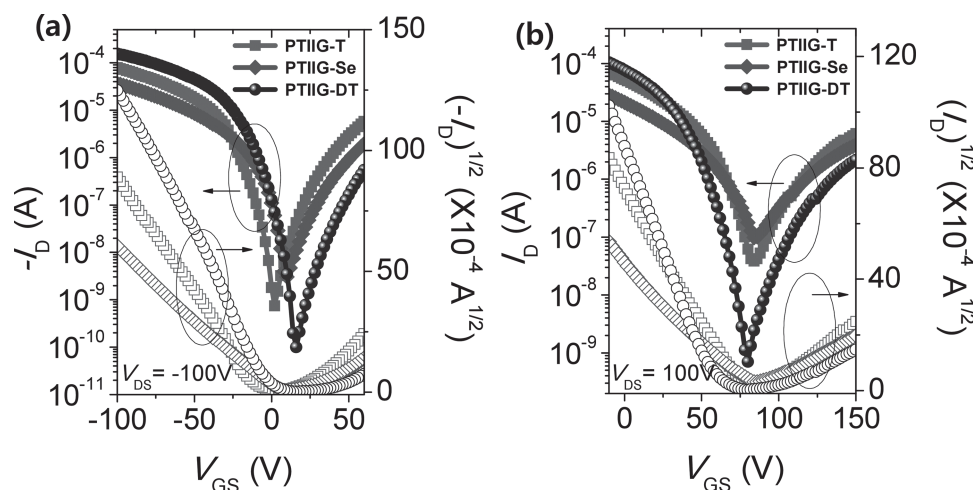
Figure 5. Transfer characteristics of OFET devices of TIIG-based polymer films annealed at 220 °C at a) hole-enhancement operation, $V_{DS} = -100V$, and b) electron-enhancement operation, $V_{DS} = +100V$ with Al electrodes.

can exhibit ambipolar charge transport upon tuning the electrode metal. It must be noted that the superior electron mobility of PTIIG-T over PTIIG-DT, despite its relatively disordered packing and conformation (vide infra), is not only observed, but also LUMO of PTIIG-T more spreads over the conjugated backbone (take a closer look at Figure 3). This suggests that the mono-thiophene (T) does not effectively act as a donor unit, but a π-conjugation between TIIG through T units is well formed, which reduces the bandgap. This phenomenon is also seen in DPP-based polymers.[14] For further enhanced performance of TIIG-based polymer OFETs with well-balanced hole and electron mobilities, we are currently studying on the optimization of ambipolar charge injections from chemically modified various metal electrodes by tuning the work function and injection barriers with the process established by Sirringhaus.[3a,15]

2.4. Microstructure Analysis

With the above results in hand, we carried out X-ray diffraction (XRD) and tapping-mode atomic force microscopy (AFM)

measurements to gain a deep insight into the structural features of the polymer thin films. As shown in **Figure 6**, the XRD patterns of PTIIG-T, PTIIG-Se, and PTIIG-DT drop-cast films showed primary diffraction peaks at 2θ of 3.75, 3.75, and
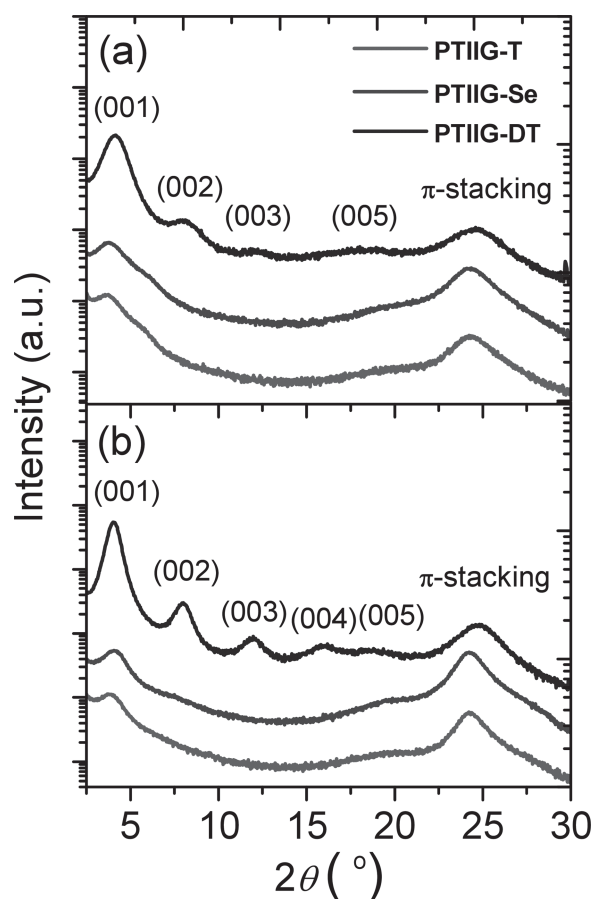
Table 3. Electrical performance of OFET devices based on annealed TIIG polymer thin films with Al contacts.

Polymer[a]	p-channel			n-channel		
	$\mu_{h,avg}$[b] [cm²V⁻¹s⁻¹]	I_{on}/I_{off}	V_T [V]	$\mu_{e,avg}$ [cm²V⁻¹s⁻¹]	I_{on}/I_{off}	V_T [V]
PTIIG-T	0.12	2.3×10^5	−11.3	1.5×10^{-2}	1.3×10^2	93.6
	(0.18)[c]			(0.03)		
PTIIG-Se	4.3×10^{-2}	8.0×10^3	−3.8	8.2×10^{-3}	4.1×10	87.1
	(4.9×10^{-2})			(9.6×10^{-3})		
PTIIG-DT	0.16	9.7×10^5	0.8	6.0×10^{-3}	3.1×10^3	102.1
	(0.28)			(9.6×10^{-3})		

[a]The polymer films were annealed at 220 °C in a nitrogen atmosphere; [b]The average mobility of the OFET devices ($L = 50$ and $W/L = 20$); [c]The maximum mobilities are shown in parenthesis.

Figure 6. Out-of-plane X-ray diffraction (XRD) patterns of TIIG-based polymer films a) as-cast and b) annealed at 220 °C.

www.MaterialsViews.com

ADVANCED
FUNCTIONAL
MATERIALS
www.afm-journal.de

FULL PAPER

Table 4. Peak assignments for out-of-plane XRD patterns.

Polymer	(00n)	As-cast		Annealed at 220 °C	
		2θ [°]	d(001)-spacing [Å]	2θ [°]	d(001)-spacing [Å]
PTIIG-T	(001)	3.75	23.52	3.77	23.39
	π-stacking[a)	24.25	3.67	24.19	3.68
PTIIG-Se	(001)	3.75	23.52	4.05	21.77
	π-stacking	24.33	3.65	24.21	3.67
PTIIG-DT	(001)	4.18	21.14	4.06	21.73
	(002)	8.07	-	8.00	-
	(003)	12.09	-	11.98	-
	(004)	-	-	16.19	-
	(005)	18.33	-	18.81	-
	π-stacking	24.56	3.62	24.80	3.59

[a)The strong and broad peaks observed at $2\theta = 24$–$25°$ in the diffraction patterns of TIIG-based polymer films are attributed to the π–π stacking.

4.18°, corresponding to d(001)-spacing values of 23.52, 23.52 and 21.14 Å (see **Table 4**). After the subsequent annealing at 220°C, the intensities of the primary peaks for both PTIIG-T and PTIIG-Se films were only slightly increased. In contrast, the primary diffraction peak of the annealed PTIIG-DT became remarkably more intense and the higher order diffraction peaks arising from the interlayer spacing reaching up to the fifth order were clearly observed, indicating a higher degree of crystallinity driven by the post-annealing process. Five highly resolved diffraction peaks were observed at $2\theta = 4.06$ (d(001) = 21.73 Å), 8.00°, 11.98°, 16.19°, and 18.81°, which indicates that

PTIIG-DT has a long-range ordered edge-on lamellar packing. Furthermore, the π–π stacking between polymer backbones in PTIIG-DT (3.59 Å) is much smaller than those observed in both the PTIIG-T and PTIIG-Se polymers ($\approx$3.68 Å), which is favorable for charge transport via hopping.

As shown in **Figure 7**, the AFM images illustrate that both the as-spun and annealed films of all the TIID-based polymers consist of uniform intertwined fiber structures that establish interconnected polymer chain networks. PTIIG-DT films form relatively fine, highly interconnected fibrillar domains with an obvious reduction of the surface roughness (RMS = 0.98 nm) when compared to the other polymers (RMS = 1.58–2.98 nm). We speculate that the more efficient charge transport in the annealed PTIIG-DT thin films is related to more densely interconnected compact domains of bundled nanofibers, which is in good agreement with the XRD and OFET results.

3. Conclusion

According to the key concept mentioned above, we have successfully synthesized a series of π-conjugated polymers containing a thienoisoindigo (TIIG) core in which the benzenes of isoindigo (IIG) block are replaced with thiophenes for high-performance OFETs. The TIIG-based polymers (PTIIG-T, PTIIG-Se, and PTIIG-DT) with electron-rich moieties (thiophene (T), selenophene (Se), or dithiophene (DT)) exhibit broad absorption bands with the edge extending up to 1600 nm, covering the whole visible to near-infrared range. All the polymers into OFETs with Au electrodes result in unipolar hole mobilities above 0.1 cm^2 V^{-1}s^{-1} and particularly, the annealed PTIIG-DT film has hole mobility of up to 0.20 cm^2 V^{-1} s^{-1} by virtue of a highly ordered lamellar structure with a short π–π stacking distance. This is the highest mobility value reported from TIIG-containing polymers. Of particular significance is that OFETs based on the polymers using Al as a cheap and low work-function electrode can tune the polarity of charge carriers, resulting in ambipolar transport characteristics capable of conducting both holes of up to 0.28 cm^2 V^{-1} s^{-1} (PTIIG-DT) and electrons of up to 0.03 cm^2 V^{-1} s^{-1} (PTIIG-T). Our results substantiate that TIIG-based polymers can operate either unipolar or ambipolar OFETs, irrespective of the counterpart co-monomer units. Further investigations of using these materials for complementary inverters and other circuits are in progress and will be reported in due course.

4. Experimental Section

Materials: All the chemicals and reagents were purchased from Sigma-Aldrich, Alfa Aesar Chemical Company, and Tokyo Chemical Industry Co., Ltd. and used without any further purification. Tetrahydrofuran (THF) was freshly dried over sodium and benzophenone, prior to use.
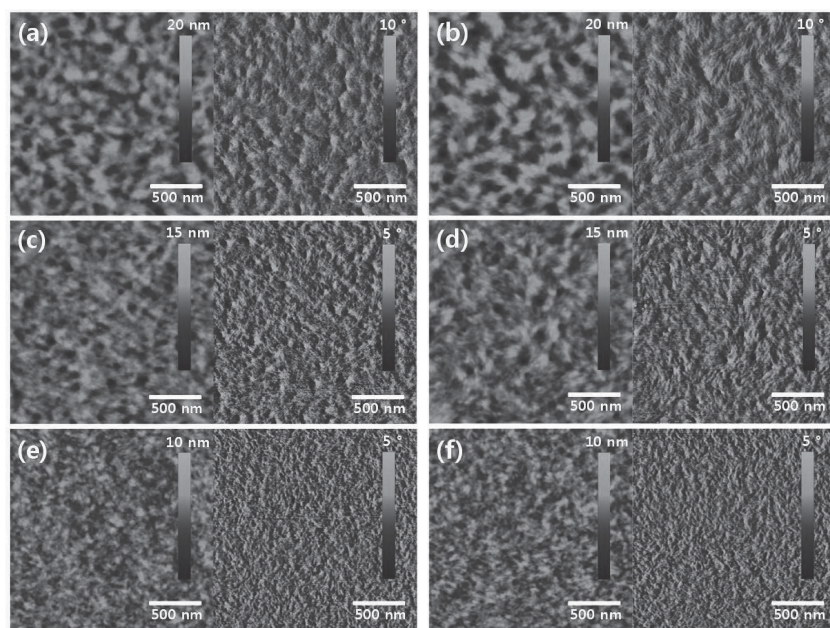

Figure 7. AFM height (left) and phase (right) images of a,b) PTIIG-T, c,d) PTIIG-Se, and e,f) PTIIG-DT. a,c,e) As cast films and b,d,e) annealed films at 220 °C on OTS-treated SiO$_2$/Si substrates.

Instruments for Characterization: ^{1}H and ^{13}C NMR were recorded on a Varian VNRS 600 MHz spectrometer using deuterated chloroform (CDCl$_3$) with tetramethylsilane (TMS) as an internal standard. Chemical shifts were given in parts per million and coupling constants (*J*) in Hertz. Elemental analyses were carried out with a Flesh 2000 elemental analyzer. The molecular weight of the polymers were determined by gel permeation chromatography (GPC) with Agilent 1200 series and miniDAWN TREOS using THF as a eluent against polysteryne (PS) standard. UV-Vis absorption spectra in solution and in thin film were recorded on a Varian Carry 5000 UV-Vis-NIR spectrophotometer. The electrochemical properties were characterized by VersaSTAT3 Princeton Applied Research Potentiostat in a three-electrode cell system with platinum as working electrode, a platinum wire counter electrode and Ag/AgCl as reference electrode. The electrolytic solution employed were 0.1 M tetra-*n*-butylammonium hexafluorophosphate (*n*-Bu$_4$NPF$_6$) in dry acetonitrile under Ar atmosphere. The reference electrode was calibrated using a ferrocene/ferrocenium redox couple as an external standard, whose oxidation potential is set at -4.8 eV with respect to zero vacuum level. The HOMO energy levels were obtained from the equation E_{HOMO} (eV) = $-$ ($E_{(ox)}^{onset}$–$E_{(ferrocene)}^{onset}$ + 4.8) (1). The LUMO levels of polymers were obtained from the equation E_{LUMO} (eV) = $-$ ($E_{(red)}^{onset}$–$E_{(ferrocene)}^{onset}$ + 4.8) (2).

General Procedure for Stille Polymerization and Polymer Purification: (*E*)-2,2'-dibromo-4,4'-bis(2-octyldodecyl)-[6,6'-bithieno[3,2-*b*]pyrrolylidene]-5,5'(4*H*,4'*H*)-dione (3) (0.250 mmol) and distannyl compound (0.250 mmol) were taken in a Schlenk tube under argon atmosphere with 10 mL of anhydrous toluene. The mixture was degassed for 20 min followed by addition of Pd$_2$(dba)$_3$ (8 mg, 8.7 μmol) and P(*o*-tolyl)$_3$ (13 mg, 42 μmol). The mixture was heated at 110 °C for 72 h. After cooling to room temperature, it was poured into methanol and the resulting precipitate was filtered. The polymer was purified by Soxhlet extraction using methanol, acetone and hexane, and finally extracted with chloroform. The chloroform solution was then concentrated by evaporation and re-precipitated in methanol. The resulting dark green colored solid was collected and dried overnight under vacuum. The polymers were characterized by ^{1}H NMR, GPC, and elemental analysis.

PTIIG-T: Isolated yield = 95%. GPC analysis M_n = 100.1 kDa, M_w = 260 kDa, and PDI = 2.60 (against PS standard).^{1}H NMR (C$_2$D$_2$Cl$_4$, 600 MHz, 353 K, δ): 7.34–7.10 (br, 2H), 6.81–6.58 (br, 2H), 4.04–3.49 (br, 4H), 2.24–1.98 (br, 2H), 1.89–1.16 (br, 64H), 1.07–0.85 (br, 12H). Anal.calcd. for C$_{56}$H$_{86}$N$_2$O$_2$S$_3$: C 73.31, H 9.67, N 3.05, O 3.49, S 10.48; found: C 73.20, H 9.53, N 2.94, S 10.32.

PTIIG-Se: Isolated yield = 90%. GPC analysis M_n = 76.3 kDa, M_w = 203 kDa, and PDI = 2.67 (against PS standard), ^{1}H NMR (C$_2$D$_2$Cl$_4$, 600 MHz, 353 K, δ): 7.46-7.20 (br, 2H), 6.74-6.48 (br, 2H), 4.02-3.52 (br, 4H), 2.19-1.98 (br, 2H), 1.88-1.15 (br, 64H,), 1.08-0.83 (br, 12H). Anal. Calcd. for C$_{56}$H$_{86}$N$_2$O$_2$S$_2$Se: C 69.74, H 9.20, N 2.90, O 3.32, S 6.65, Se, 8.19; found: C 69.61, H 9.02, N 2.71, S, 6.68.

PTIIG-DT: Isolated yield = 92%. GPC analysis M_n = 77.1 kDa, M_w = 161 kDa, and PDI = 2.08 (against PS standard). ^{1}H NMR (C$_2$D$_2$Cl$_4$, 600 MHz, 353 K, δ): 7.38–6.89 (br, 4H), 6.78–6.49 (br, 2H), 4.04–3.48 (br, 4H), 2.14–1.12 (br, 66H), 1.09–0.81 (br, 12H). Anal. Calcd. for C$_{60}$H$_{88}$N$_2$O$_2$S$_4$: C 72.09, H 9.07, N 2.80, O 3.20, S 12.83; found: C 71.55, H 8.85, N 2.66, S12.44.

OFET Fabrication and Testing: OFETs with bottom-gate top-contact configuration were prepared to characterize the electrical performance of TIIG-based polymers. A highly *n*-doped (100) Si wafer (< 0.004 Ω cm) with a thermally grown SiO$_2$ (300 nm, C_i = 10 nF cm^{-2}) was utilized as the substrate and dielectrics and the SiO$_2$ surface was modified with *n*-octadecyltrimethoxysilane (OTS) self-assembled monolayer (SAM) as previously reported.[16] 3 mM of OTS solution in trichloroethylene was spin-coated on the piranha-solution-cleaned wafer at 3000 rpm for 30 s. Then, the wafer was exposed to ammonia vapor for ≈12 h, followed by sonication cleaning, sequential washing, and drying. The contact angle (DI water) on the hydrophobic OTS-modified wafer was ≈110°. TIIG-based polymers were dissolved in *o*-DCB (3 mg mL^{-1}) and the film of TIIG-based polymers was prepared on the substrate by drop-casting. Either Au or Al contacts (40 nm) were thermally evaporated onto the

polymer film to form source and drain electrodes with a channel length (*L*) of 50 μm and a channel width (*W*) of 1000 μm using shadow mask. The electrical performance of OFETs was measured in a N$_2$-filled glove box using a Keithley 4200 semiconductor parametric analyzer. The field-effect mobility was calculated in the saturation regime using the following equation:

$$I_{DS} = \frac{1}{2}(W/L)\mu C_i(V_G - V_T)^2 \qquad (3)$$

where I_{DS} is the drain-to-source current, μ is the mobility, and V_G and V_T are the gate voltage and threshold voltage, respectively.

Supporting Information

Supporting Information is available from the Wiley Online Library or from the author.

Acknowledgements

[1] a) H. Sirringhaus, N. Tessler, R. H. Friend, *Science* **1998**, *280*, 1741; b) Z. Bao, *Adv. Mater.* **2000**, *12*, 227; c) M. Zhang, H. N. Tsao, W. Pisula, C. Yang, A. K. Mishra, K. Müllen, *J. Am. Chem. Soc.* **2007**, *129*, 3472; d) Z. Bao, Y. Feng, A. Dodabalapur, V. R. Raju, A. J. Lovinger, *Chem. Mater.* **1997**, *9*, 1299; e) S. Wang, M. Kappl, I. Liebewirth, M. Müller, K. Kirchhoff, W. Pisula, K. Müllen, *Adv. Mater.* **2012**, *24*, 417; f) H. Yan, Z. Chen, Y. Zheng, C. Newman, J. R. Quinn, F. Dötz, M. Kastler, A. Facchetti, *Nature* **2009**, *457*, 679; g) A. Facchetti, *Chem. Mater.* **2010**, *23*, 733; h) H. Sirringhaus, T. Kawase, R. H. Friend, T. Shimoda, M. Inbasekaran, W. Wu, E. P. Woo, *Science* **2000**, *290*, 2123; i) P. M. Beaujuge, J. M. J. Fréchet, *J. Am. Chem. Soc.* **2011**, *133*, 20009; j) I. McCulloch, M. Heeney, C. Bailey, K. Genevicius, I. MacDonald, M. Shkunov, D. Sparrowe, S. Tierney, R. Wagner, W. Zhang, M. L. Chabinyc, R. J. Kline, M. D. McGehee, M. F. Toney, *Nat. Mater.* **2006**, *5*, 328; k) S. C. B. Mannsfeld, A. Sharei, S. Liu, M. E. Roberts, I. McCulloch, M. Heeney, Z. Bao, *Adv. Mater.* **2008**, *20*, 4044.

[2] a) A. B. Tamayo, B. Walker, T.-Q. Nguyen, *J. Phys. Chem. C* **2008**, *112*, 11545; b) E. Zhou, S. Yamakawa, K. Tajima, C. Yang, K. Hashimoto, *Chem. Mater.* **2009**, *21*, 4055; c) L. Bürgi, M. Turbiez, R. Pfeiffer, F. Bienewald, H.-J. Kirner, C. Winnewisser, *Adv. Mater.* **2008**, *20*, 2217; d) J. Lee, A.-R. Han, J. Kim, Y. Kim, J. H. Oh, C. Yang, *J. Am. Chem. Soc.* **2012**, *134*, 20713; e) J. Lee, S. Cho, J. H. Seo, P. Anant, J. Jacob, C. Yang, *J. Mater. Chem.* **2012**, *22*, 1504; f) M. M. Wienk, M. Turbiez, J. Gilot, R. A. J. Janssen, *Adv. Mater.* **2008**, *20*, 2556; g) S. Cho, J. Lee, M. Tong, J. H. Seo, C. Yang, *Adv. Funct. Mater.* **2011**, *21*, 1910; h) L. Huo, J. Hou, H.-Y. Chen, S. Zhang, Y. Jiang, T. L. Chen, Y. Yang, *Macromolecules* **2009**, *42*, 6564; i) J. Lee, A.-R. Han, J. Hong, J. H. Seo, J. H. Oh, C. Yang, *Adv. Funct. Mater.* **2012**, *22*, 4128; j) J. Lee, S. Cho, C. Yang, *J. Mater. Chem.* **2011**, *21*, 8528.

[3] a) Z. Chen, M. J. Lee, R. Shahid Ashraf, Y. Gu, S. Albert-Seifried, M. Meedom Nielsen, B. Schroeder, T. D. Anthopoulos, M. Heeney, I. McCulloch, H. Sirringhaus, *Adv. Mater.* **2012**, *24*, 647; b) J. Mei, K. R. Graham, R. Stalder, J. R. Reynolds, *Org. Lett.* **2010**, *12*, 660; c) R. Stalder, J. Mei, J. R. Reynolds, *Macromolecules* **2010**, *43*, 8348; d) L. Biniek, B. C. Schroeder, C. B. Nielsen, I. McCulloch, *J. Mater. Chem.* **2012**, *22*, 14803; e) H. Bronstein, Z. Chen, R. S. Ashraf, W. Zhang, J. Du, J. R. Durrant, P. Shakya Tuladhar, K. Song, S. E. Watkins, Y. Geerts, M. M. Wienk, R. A. J. Janssen, T. Anthopoulos, H. Sirringhaus, M. Heeney, I. McCulloch, *J. Am. Chem. Soc.* **2011**, *133*, 3272; f) R. Stalder, J. Mei, J. Subbiah, C. Grand, L. A. Estrada, F. So, J. R. Reynolds, *Macromolecules* **2011**, *44*, 6303.

[4] a) T. Lei, Y. Cao, Y. Fan, C.-J. Liu, S.-C. Yuan, J. Pei, *J. Am. Chem. Soc.* **2011**, *133*, 6099; b) Y. Li, S. P. Singh, P. Sonar, *Adv. Mater.* **2010**, *22*, 4862; c) E. Wang, Z. Ma, Z. Zhang, P. Henriksson, O. Inganäs, F. Zhang, M. R. Andersson, *Chem. Commun.* **2011**, *47*, 4908; d) J. Mei, D. H. Kim, A. L. Ayzner, M. F. Toney, Z. Bao, *J. Am. Chem. Soc.* **2011**, *133*, 20130; e) J. C. Bijleveld, A. P. Zoombelt, S. G. J. Mathijssen, M. M. Wienk, M. Turbiez, D. M. de Leeuw, R. A. J. Janssen, *J. Am. Chem. Soc.* **2009**, *131*, 16616; f) E. Wang, Z. Ma, Z. Zhang, K. Vandewal, P. Henriksson, O. Inganäs, F. Zhang, M. R. Andersson, *J. Am. Chem. Soc.* **2011**, *133*, 14244; g) T. Lei, J.-H. Dou, J. Pei, *Adv. Mater.* **2012**, *24*, 6457; h) T. Lei, J.-H. Dou, Z.-J. Ma, C.-H. Yao, C.-J. Liu, J.-Y. Wang, J. Pei, *J. Am. Chem. Soc.* **2012**, *134*, 20025.

[5] X. Guo, N. Zhou, S. J. Lou, J. W. Hennek, R. Ponce Ortiz, M. R. Butler, P.-L. T. Boudreault, J. Strzalka, P.-O. Morin, M. Leclerc, J. T. López Navarrete, M. A. Ratner, L. X. Chen, R. P. H. Chang, A. Facchetti, T. J. Marks, *J. Am. Chem. Soc.* **2012**, *134*, 18427.

[6] R. S. Ashraf, A. J. Kronemeijer, D. I. James, H. Sirringhaus, I. McCulloch, *Chem. Commun.* **2012**, *48*, 3939.

[7] Y. Koizumi, M. Ide, A. Saeki, C. Vijayakumar, B. Balan, M. Kawamoto, S. Seki, *Polym. Chem.* **2013**, *4*, 484.

[8] G. W. P. Van Pruissen, F. Gholamrezaie, M. M. Wienk, R. A. J. Janssen, *J. Mater. Chem.* **2012**, *22*, 20387.

[9] a) K. Watanabe, I. Osaka, S. Yorozuya, K. Akagi, *Chem. Mater.* **2012**, *24*, 1011; b) S. Haid, A. Mishra, M. Weil, C. Uhrich, M. Pfeiffer, P. Bäuerle, *Adv. Funct. Mater.* **2012**, *22*, 4322.

[10] T. Lei, Y. Cao, X. Zhou, Y. Peng, J. Bian, J. Pei, *Chem. Mater.* **2012**, *24*, 1762.

[11] J. C. Bijleveld, R. A. M. Verstrijden, M. M. Wienk, R. A. J. Janssen, *J. Mater. Chem.* **2011**, *21*, 9224.

[12] a) M. Shahid, T. McCarthy-Ward, J. Labram, S. Rossbauer, E. B. Domingo, S. E. Watkins, N. Stingelin, T. D. Anthopoulos, M. Heeney, *Chem. Sci.* **2012**, *3*, 181; b) B. Kim, H. R. Yeom, M. H. Yun, J. Y. Kim, C. Yang, *Macromolecules* **2012**, *45*, 8658.

[13] a) H. Dong, L. Jiang, W. Hu, *Phys. Chem. Chem. Phys.* **2012**, *14*, 14165; b) S. Ogawa, Y. Kimura, M. Niwano, H. Ishii, *Appl. Phys. Lett.* **2007**, *90*, 033504; c) M. Kraus, S. Richler, A. Opitz, W. Brutting, S. Haas, T. Hasegawa, A. Hinderhofer, F. Schreiber, *J. Appl. Phys.* **2010**, *107*, 094503.

[14] W. Li, W. S. C. Roelofs, M. M. Wienk, R. A. J. Janssen, *J. Am. Chem. Soc.* **2012**, *134*, 13787.

[15] a) X. Cheng, Y.-Y. Noh, J. Wang, M. Tello, J. Frisch, R.-P. Blum, A. Vollmer, J. P. Rabe, N. Koch, H. Sirringhaus, *Adv. Funct. Mater.* **2009**, *19*, 2407; b) M. C. Gwinner, S. Khodabakhsh, H. Giessen, H. Sirringhaus, *Chem. Mater.* **2009**, *21*, 4425.

[16] a) A. Virkar, S. Mannsfeld, J. H. Oh, M. F. Toney, Y. H. Tan, G.-y. Liu, J. C. Scott, R. Miller, Z. Bao, *Adv. Funct. Mater.* **2009**, *19*, 1962; b) Y. Ito, A. A. Virkar, S. Mannsfeld, J. H. Oh, M. Toney, J. Locklin, Z. Bao, *J. Am. Chem. Soc.* **2009**, *131*, 9396.